ACS APPLIED MATERIALS & INTERFACES

Research Article

www.acsami.org

Multiplexed Gas Sensor Based on Heterogeneous Metal Oxide Nanomaterial Array Enabled by Localized Liquid-Phase Reaction

Daejong Yang,[†,‡] M. Kasyful Fuadi,[†,‡] Kyungnam Kang,[†,‡] Donghwan Kim,[†,§] Zhiyong Li,[∥] and Inkyu Park*[,†,‡]

[†]Mechanical Engineering Department, Korea Advanced Institute of Science and Technology (KAIST), Daejeon 305-701, South Korea

[‡]KI for the NanoCentury, Korea Advanced Institute of Science and Technology (KAIST), Daejeon 305-701, South Korea

[§]Korea Electric Power Research Institute (KEPRI), Korea Electric Power Corporation (KEPCO), Daejeon 300-760, South Korea

[∥]Systems Research Lab, Hewlett-Packard Laboratory, Palo Alto, California 94304-1126, United States

Supporting Information

ABSTRACT: A novel method for the selective and localized synthesis of nanomaterials and their in situ integration based on serial combination of localized liquid-phase reaction has been developed for the fabrication of heterogeneous nanomaterial array. This method provides simple, fast and cost-effective fabrication process by using well-controlled thermal energy and therefore solves the challenging problems of assembly and integration of heterogeneous nanomaterial array in functional microelectronic devices. We have fabricated a parallel array of TiO_2 nanotubes, CuO nanospikes, and ZnO nanowires, which exhibited adequate gas sensing response. Furthermore, we could approximately determine individual gas concentrations in a mixture gas consisting of 0−2 ppm of NO_2 and 0−800 ppm of CO gas species by analyzing multiple data from an array of heterogeneous sensing nanomaterials.

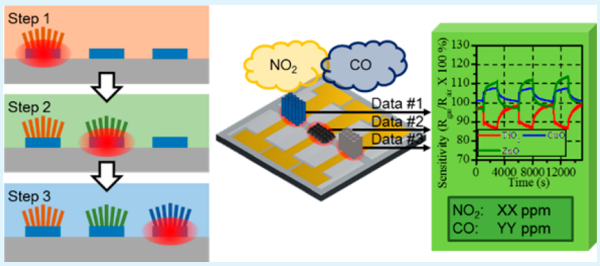

KEYWORDS: *heterogeneous nanomaterial array, mixture gas sensor, local synthesis, semiconductor nanomaterial, one-dimensional nanomaterial*

INTRODUCTION

Since it was found that the electrical properties of metal oxide semiconductors (e.g., ZnO and SnO_2 thin films) are sensitive to the chemical composition of surrounding atmosphere,[1,2] metal oxide semiconductor based gas sensors have been widely developed because of their simple design and cost-effective detection scheme for various gases.[3−5] However, because of their nonspecific reactions with various reducing or oxidizing gases,[6] filter embedded devices have to be used to reduce the cross-sensitivity to interfering gases. The filters absorb certain interfering gases, convert certain interfering gases to non-reacting gases or block undesired large molecule gases.[7−9] However, the filters cannot work on unexpected interfering gases and should be replaced regularly because of the damage and contamination by interfering gases. Another approach to improve the selectivity of gas sensing system is to use an array of multiple gas sensors. K. Persaud et al. introduced a system consisting of three different commercial sensors and showed accurate odor sensing performance by combining and analyzing multiple data from the sensor array.[10] Although multiple sensor array can improve the sensitivity and selectivity of sensing systems, as well as classify gas components in mixture gases, their applications are limited due to their large size, high power consumption and high manufacturing cost.[11−15]

Recently, one-dimensional (1D) nanomaterials have been widely researched for gas sensor applications because of their high sensitivity, fast response, small size, and low power consumption. This can be attributed to their high surface reactivity, large surface to volume ratio and small radius comparable to the Debye length.[16,17] To better utilize these advantages of 1D nanomaterials, their highly integrated and multiplexed array should be developed. Recently, several small-sized nanomaterial array sensors have been developed by using traditional sensor fabrication methods, such as screen printing,[18] inkjet printing,[19] and drop casting.[20] However, these methods provided only limited resolution and alignment accuracy for patterning on microelectronic devices. Alternative methods for the integration and patterning of 1D nanomaterials, such as dielectrophoresis,[21] contact printing,[22] and focused ion beam (FIB)[23] based bonding process, have been developed for the integrated sensor array fabrication. However, they have several drawbacks such as poor controllability, low throughput or weak contact between electrode and sensing materials.

Received: January 6, 2015
Accepted: April 22, 2015
Published: April 22, 2015

DOI: 10.1021/acsami.5b00110
ACS Appl. Mater. Interfaces 2015, 7, 10152−10161

To overcome these problems and to realize high-performance multiplexed gas sensor array, we developed an alternative hybrid nanofabrication method for the controlled synthesis of functional nanomaterials based on hydrothermal reaction[24,25] and liquid phase deposition (LPD)[26] at localized and selected locations enabled by thermal energy control. Scheme 1 shows the basic principle of this method. A localized temperature increase at Joule-heated microheaters within liquid precursor results in the convective mass flux of precursor to the microheater, at which direct synthesis and integration of nanomaterials occur. A serial combination of this process by using different microheaters and liquid precursors realizes an array of heterogeneous nanomaterials (see Scheme 1a). No cross-contamination between nanomaterials or their damages occur by choosing proper sequence of precursor liquid and thorough rinsing between each step. This kind of highly integrated and multiplexed array of different functional materials can be used for advanced engineering applications such as multiplexed chemical sensor array for multicomponent gas analytes (see Scheme 1b).

Scheme 1. (a) Heterogeneous Nanomaterial Array Fabrication by Series of Localized Liquid-Phase Synthesis[a] and (b) Multiplexed Gas Sensor Based on Heterogeneous Nanomaterial Array Used for Multi-Component Gas Sensing

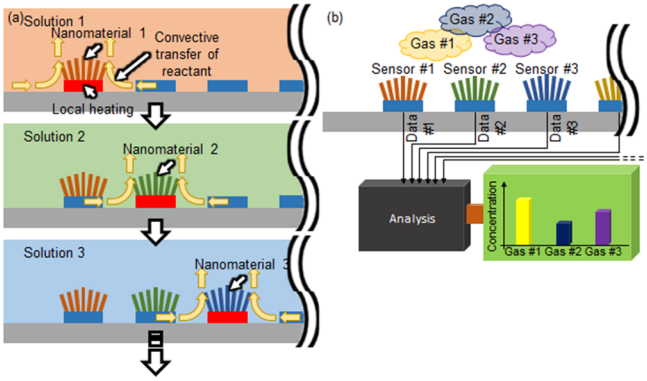

[a]The nanomaterials are selectively and locally synthesized at the targeted spots by localized thermal energy control in different liquid precursor environments.

In this work, we realized the fabrication of multiplexed array of heterogeneous nanomaterials by using the propose method; As a proof-of-concept, we have fabricated an array of CuO nanospikes, ZnO nanowires, and TiO_2 nanotubes that are common materials for gas sensing applications.[27] In addition, we have employed a simple graphical method for quick and easy quantification of multicomponent gas analytes with much less computational cost. Previously developed methods for multicomponent sensors including principal component analysis (PCA), redundancy analysis (RDA), artificial neural networks (ANNS), etc., are not suitable for nonlinear equations or computationally intensive for real-time gas sensing applications. On the other hand, graphical method has been widely used for simple numerical solution of simultaneous nonlinear equations.[28] In this work, three nonlinear equations obtained from different sensor signals were utilized to find concentrations of two individual gas components. Since the number of equations is larger than the number of unknowns, we estimated the gas concentrations by using the incenter of the triangle formed by three equations. In specific, we could easily detect the concentrations of NO_2 and CO gases in their single component or mixture samples by using the multiple sensing signals from the array of heterogeneous sensing materials and simple graphical analysis.

MATERIALS AND METHODS

Design and Fabrication of Microheater Devices. Two kinds of microheater embedded devices were used in this work: devices with single embedded microheater and devices with three embedded microheaters. Both devices were fabricated by conventional microfabrication processes. Photoresist (PR; AZ5214, MicroChemicals GmbH, Germany) was patterned on a Si wafer with 2 μm thick thermal oxide by photolithography process. A 10 nm thick titanium (Ti) adhesion layer and 200 nm thick platinum (Pt) film were deposited on the substrate by e-beam evaporation and PR layer and dummy Pt film were lifted-off in acetone to obtain Pt microheater. Then, a 600 nm thick silicon dioxide (SiO_2) layer was deposited on the substrate by plasma enhanced chemical vapor deposition (PECVD) at 250 °C for the electrical insulation. Then, PR was patterned again on the SiO_2 layer to fabricate interdigitated electrodes by aligning with underlying microheaters. A 10 nm thick chrome (Cr) adhesion layer and 200 nm thick gold (Au) film were deposited on the substrate by e-beam evaporation and lift-off process was carried out to define interdigitated electrodes.

Synthesis of Nanomaterials. Three kinds of precursor solutions were used in this work: CuO nanospike precursor, ZnO nanowire precursor, and TiO_2 nanotube precursor solutions. The CuO precursor solution consists of 4 mM copper(II) nitrate hydrate ($Cu(NO_3)_2{\cdot}xH_2O$) and 4 mM hexamethylenetetramine (HMTA, $C_6H_{12}N_4$) in DI water; ZnO precursor solution consists of 25 mM zinc nitrate hexahydrate ($Zn(NO_3)_2{\cdot}6H_2O$), equimolar HMTA and 6 mM polyethylenimine (PEI) in DI water; and TiO_2 precursor solution consists of 0.3 M boric acid (H_3BO_3) and 0.1 M ammonium hexafluorotitanate ($(NH_4)_2TiF_6$) in DI water. (All chemicals were purchased from Sigma-Aldrich.) To synthesize single-type nanomaterials, a small PDMS well was attached on the single microheater embedded device and 0.01 mL of CuO or ZnO precursor solution were dispensed in the well. A DC bias of 1.9 V was applied to the microheater for 5 and 60 min to synthesize CuO nanospikes and ZnO nanowires, respectively. To synthesize TiO_2 nanotubes, 0.01 mL of TiO_2 precursor solution was supplied to presynthesized ZnO nanowire templates. After 15 min, TiO_2 precursor solution was removed and the device was washed in DI water. To synthesize heterogeneous nanomaterial arrays, devices with three embedded microheater array were used. The fabrication process consisted of four steps: (1) CuO nanospike synthesis, (2) ZnO nanowire synthesis, (3) conversion of ZnO nanowires to TiO_2 nanotubes, and (4) ZnO nanowire synthesis. First, a small PDMS well was attached on the device. 0.01 mL of CuO precursor solution was dispensed in the well and 1.9 V DC bias was applied to the microheater 2 for 5 min. Then, 0.01 mL of ZnO precursor solution was dispensed and the same electrical bias was applied to the microheater 1 for 60 min. Afterward, 0.01 mL of TiO_2 precursor solution was supplied for 15 min without any heating. In the last step, 0.01 mL of ZnO precursor solution was supplied again and the same electrical bias was applied to the microheater 3 for 60 min. The device was thoroughly washed with DI water after each step in order to prevent the chemical contamination between different nanomaterials.

Mixture Gas Sensing Test. The heterogeneous nanomaterial array device was located in the test chamber and various concentrations of NO_2 and CO mixture gas were supplied into the chamber by controlling the flow rates of air balanced target gas and air with mass flow controllers (MFCs). An electrical power for microheater was applied by using a DC power supply (E3642A, Agilent) and the resistances of three sensing materials were simultaneously measured by source meters (2400 and 2636B, Keithley).

DOI: 10.1021/acsami.5b00110
ACS Appl. Mater. Interfaces 2015, 7, 10152−10161

RESULTS AND DISCUSSION

To fabricate an array of heterogeneous nanomaterials in small areas for highly integrated sensor device, we have employed local hydrothermal reaction by using device platform with embedded microheaters (see Supporting Information Figure S1 for the detail of device). Various kinds of nanomaterials can be locally synthesized at the targeted area. Figure 1a shows the

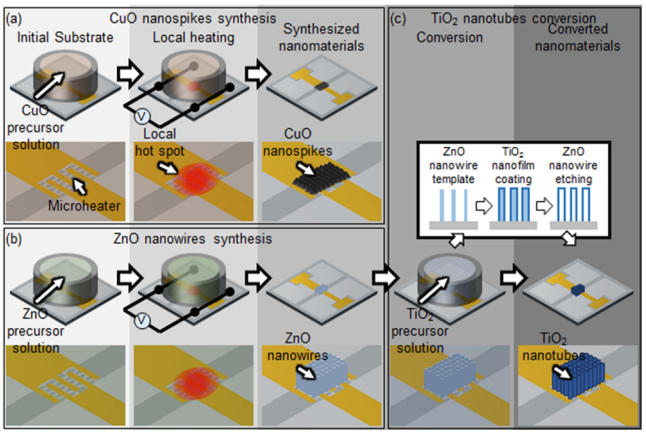

Figure 1. Process flow for nanomaterial synthesis. Schematics of localized hydrothermal synthesis process for (a) CuO nanospikes and (b) ZnO nanowires. (c) Schematics of liquid phase deposition process for the TiO_2 nanotubes with presynthesized ZnO nanowire template. CuO nanospikes and ZnO nanowires are selectively synthesized on the locally heated areas by using microheater. TiO_2 nanotubes are synthesized by room-temperature liquid phase deposition on the ZnO nanowire template and simultaneous removal of ZnO nanowires in acidic environment.

schematic of localized hydrothermal synthesis of metal oxide nanomaterials. When a metal oxide precursor solution is supplied and an electrical bias is applied across the embedded microheater, the local hot spot is generated by Joule heating and the temperature of precursor solution is locally increased near the microheater. The nanomaterials are synthesized on the electrodes by endothermic reaction. The fresh precursor solution is continuously supplied with a convective flow induced by local heating and nanomaterials continue to grow during the reaction period. The nanomaterials make reliable bonding with electrodes because they are directly synthesized on the electrodes. The nanomaterials grown on the interdigitated electrode pairs are connected with each other, making an electrical interconnection for the device. More specifically, Figure 1a and 1b shows the schematics of synthesis process of CuO nanospikes and ZnO nanowires. The precursor solutions for CuO nanospikes or ZnO nanowires are supplied in a small liquid container and electrical bias is applied across the microheater. The CuO nanospikes or ZnO nanowires are locally synthesized at the designated areas. As shown in Figure 1c, TiO_2 nanotubes are synthesized by additional LPD of TiO_2 layer along the surface of presynthesized ZnO nanowire templates. The tubular structure of TiO_2 is formed because of the in situ etching of ZnO nanowire template under low pH environment of TiO_2 precursor while TiO_2 layer is formed on the surface.[27] Figure 2 shows the scanning electron microscopy (SEM) images, transmission electron microscopy (TEM) images and electron dispersive spectroscopy (EDS) data of CuO nanospikes (Figure 2a–e), ZnO nanowires (Figure 2f–j), and TiO_2 nanotubes (Figure 2k–o). The size of nanomaterials varies by the location because of the temperature variation near the microheater. The average length of ZnO nanowires at the center of the nanowire bundle is ~6 μm but dramatically shortens at the edge. The average diameter of ZnO nanowires is ~50 nm and almost independent from the location since the PEI functioned as side wall capping agent.[29,30] However, several thicker nanowires can be observed due to the fusion of adjacent nanowires during the synthesis process. TiO_2 shows tubular nanostructures with thickness of 20–50 nm and inner diameter similar to those of ZnO nanowires. The height and diameter of CuO nanospikes are approximately 2 μm and 200 nm, respectively. Because of low thermal conductivity of nanosized CuO,[31] heat could not be effectively transferred along the longitudinal direction and nanospikes were synthesized with uniform lengths on the entire microheater. The HRTEM images of CuO nanospike (Figure 2e) and ZnO nanowire (Figure 2j) exhibit that spaces between two neighboring fringes are 0.27 and 0.52 nm corresponding to the distance of the [110] and [0001] plane of CuO[32] and ZnO,[33] respectively. As shown in the SEM and TEM images of TiO_2 nanotubes (Figure 2l, n, and o), they were synthesized as tubular structure with no specific crystallinity. (see Materials and Methods section and Supporting Information for details about the synthesis process of nanomaterials)

Multiplexed array of heterogeneous nanomaterials can be fabricated by the sequential combination of above-mentioned synthesis processes. To synthesize an array of heterogeneous nanomaterials on a single chip, a device platform embedded with three individual microheaters were fabricated by using the same conventional microfabrication process as the single microheater device. The dimensions of individual microheaters are the same as those of single microheater device and each microheaters are separated by 200 μm to avoid the thermal effect by the neighboring microheaters (Figure 3a). Figure 3b–d shows the infrared (IR) image of microheater array, while 3.5 V of electrical bias was applied to the first, second and third microheater, respectively. The temperatures of targeted microheaters were locally raised and the IR image of these regions got immediately brightened. As shown in Supporting Information Figure S2a and b, the microheater was rapidly heated and cooled within 0.03 s because of the small heat capacity.[34] The temperature profile on chip obtained by numerical simulation also verifies highly localized heating. As shown in the numerical simulation results (Figure 3e and g), the temperature increase is highly localized and does not affect neighboring regions. The temperature at the heating zone is estimated to be 300–350 °C by the measurement of microheater resistance as well as by numerical simulation. Figure 3f and h shows the numerical simulation results of temperature profile during nanomaterial synthesis process in the aqueous precursor solution, in which the temperature is also locally increased to the synthesis temperature (85–95 °C) on the selected microheater. Supporting Information Figure S3a–f shows the temperature profile of the chip while electrical bias was applied to all three microheaters in the air and the precursor solution, respectively. The temperature is also locally increased near the microheaters and the heat is not spread to the surroundings. As shown in the cross-sectional temperature distribution (Supporting Information Figure S3e and f), high temperature regions are isolated in the insulation layer composed of SiO_2 because of its low thermal conductivity.[35] The SiO_2 insulation layer reduces the heat transfer to the bottom direction, thereby the heat can be efficiently used for

DOI: 10.1021/acsami.5b00110
ACS Appl. Mater. Interfaces 2015, 7, 10152–10161

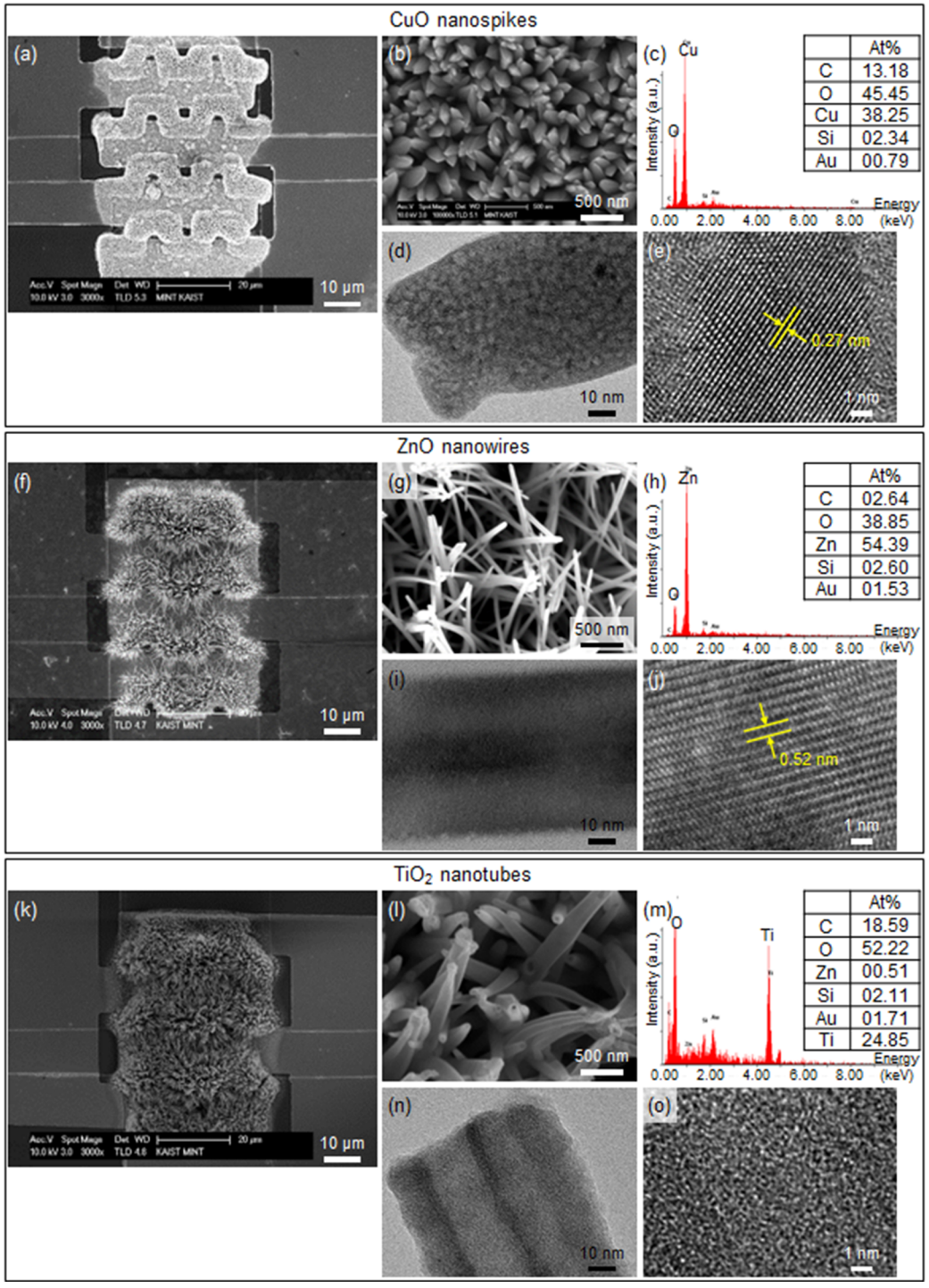

Figure 2. Surface characterization of locally synthesized nanomaterials: SEM images of (a, b) CuO nanospikes, (f, g) ZnO nanowires, and (k, l) TiO_2 nanotubes; EDS data of (c) CuO nanospikes, (h) ZnO nanowires, and (m) TiO_2 nanotubes; TEM images of (d, e) CuO nanospikes, (i, j) ZnO nanowires, and (n, o) TiO_2 nanotubes. The results show that each nanostructure was successfully synthesized on desired location by either localized hydrothermal synthesis (CuO nanospikes and ZnO nanowires) or localized liquid phase deposition (TiO_2 nanotubes).

nanomaterial synthesis (during synthesis process) and for heating the sensing materials (during sensor operation).

The fabrication process for heterogeneous nanomaterial array was designed by using serial combination of localized hydrothermal reaction (i.e., hydrothermal synthesis of CuO nanospikes and ZnO nanowires) and LPD process (i.e., synthesis of TiO_2 nanotubes). Figure 4a and b shows the schematics of fabrication process, which consists of four steps: (step1) synthesis of CuO nanospikes on microheater 2 by local heating in CuO precursor solution; (step 2) synthesis of ZnO nanowires on microheater 1 by local heating in ZnO precursor solution; (step 3) conversion of ZnO nanowires to TiO_2 nanotubes on microheater 1 at room temperature in TiO_2 precursor solution; (step 4) synthesis of ZnO nanowires on microheater 3 by local heating in ZnO precursor solution. Details of process parameters and procedures were already

DOI: 10.1021/acsami.5b00110
ACS Appl. Mater. Interfaces 2015, 7, 10152−10161

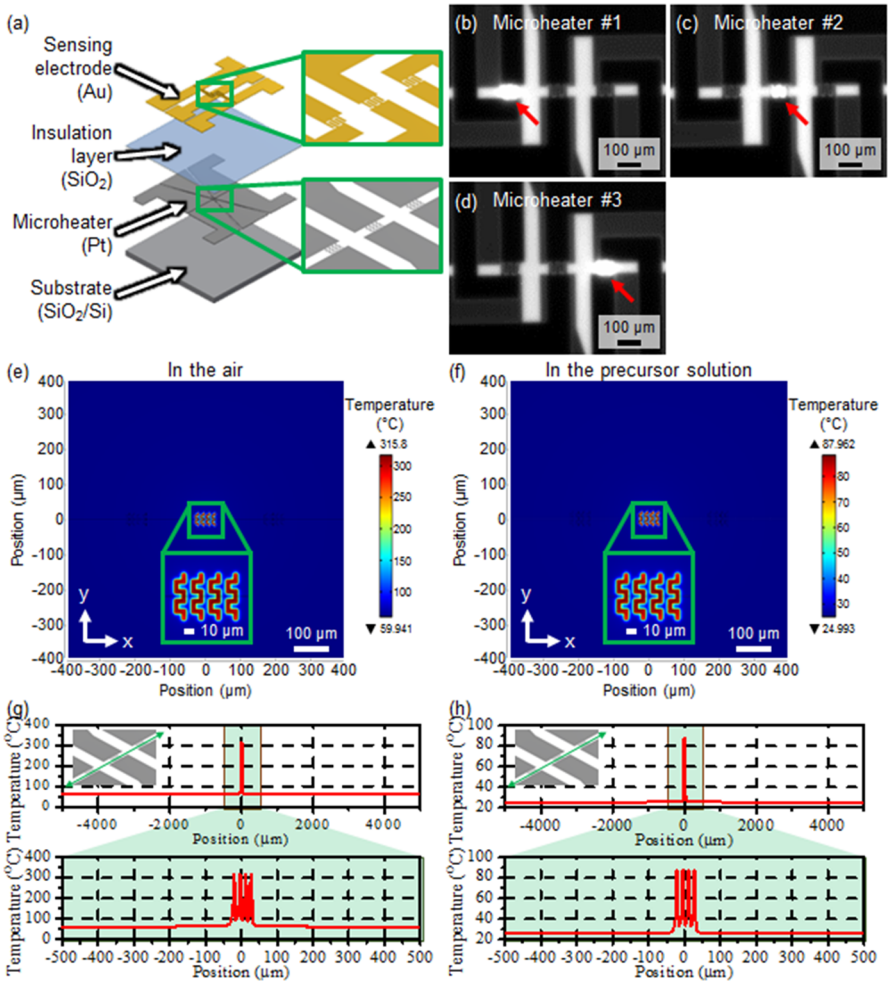

Figure 3. (a) Schematic of the sensor array device consisting of three microheaters, insulation layer, and three pairs of interdigitated sensing electrodes. (b–d) Infrared image of sensor array during local heating at the microheaters 1–3, respectively, under 3.5 V of DC bias; Temperature profile of the microheater array device in (e) the air and (f) the precursor solution by numerical simulation; Temperature-position curve along the center line of the microheater array device in (g) the air and (h) the precursor solution. Here, 3.5 and 1.9 V of DC bias were applied to microheater for Joule-heating in the air and the precursor solution, respectively.

explained in the Synthesis of Nanomaterials section. To minimize the cross-contamination between different nanomaterials, the sample chip was thoroughly rinsed with deionized (DI) water after each synthesis step. Figure 4c shows the SEM images of the device after each synthesis step. Although all three electrodes were exposed to the CuO precursor solution in step 1 and to the ZnO precursor solution in step 2 and 4, the target nanomaterials were synthesized only at the desired location in each synthesis step by localized temperature control with individual microheaters. Supporting Information Figure S4 shows the SEM images of nanomaterials after each synthesis step and Figure 4d–i shows the high resolution SEM images and EDS data of finally synthesized nanomaterials. The ZnO nanowires were successfully converted to the TiO_2 nanotubes and the shape of other nanomaterials were not changed during successive synthesis processes. The geometrical parameters (shape, average diameter, and length) of TiO_2 nanotubes, CuO nanospikes and ZnO nanowires were almost identical to those of individually synthesized materials on the single microheater devices. The EDS data indicates that TiO_2 nanotubes contain only small percentages of Zn elements remained after the conversion process in step 3. Also, the EDS spectra data from the CuO nanospikes and ZnO nanowires show the purity of synthesized materials without detectable cross-contamination (Supporting Information Figure S5).

The heterogeneous nanomaterial array consisting of TiO_2 nanotubes, CuO nanospikes and ZnO nanowires can be used as a multiplexed sensor for the multicomponent gases. The adsorption/desorption of gas molecules and corresponding change of surface potential are the essential principle for the resistive type metal oxide based semiconductor gas sensors. In the atmospheric condition, oxygen molecules are adsorbed on the surface of metal oxide materials and form negative oxygen ions (O^-) by capturing electrons from the material. The charge carriers of n-type materials (e.g., TiO_2 nanotubes and ZnO nanowires) are electrons and those of p-type materials (e.g., CuO nanospike) are holes.[36,37] When metal oxide materials are exposed to the oxidizing gas (e.g., NO_2), oxygen ions formed from the oxidizing gas are adsorbed on the surface of sensing materials by capturing electrons. As a result, free electron density within n-type materials is decreased and hole density within p-type materials is increased.[38−40] On the contrary, when reacting with reducing gas (e.g., CO), oxygen ions are desorbed from the surface of metal oxide and free electrons are returned to the metal oxide. Therefore, the electron density in n-type materials is increased and hole density in p-type

DOI: 10.1021/acsami.5b00110
ACS Appl. Mater. Interfaces 2015, 7, 10152−10161

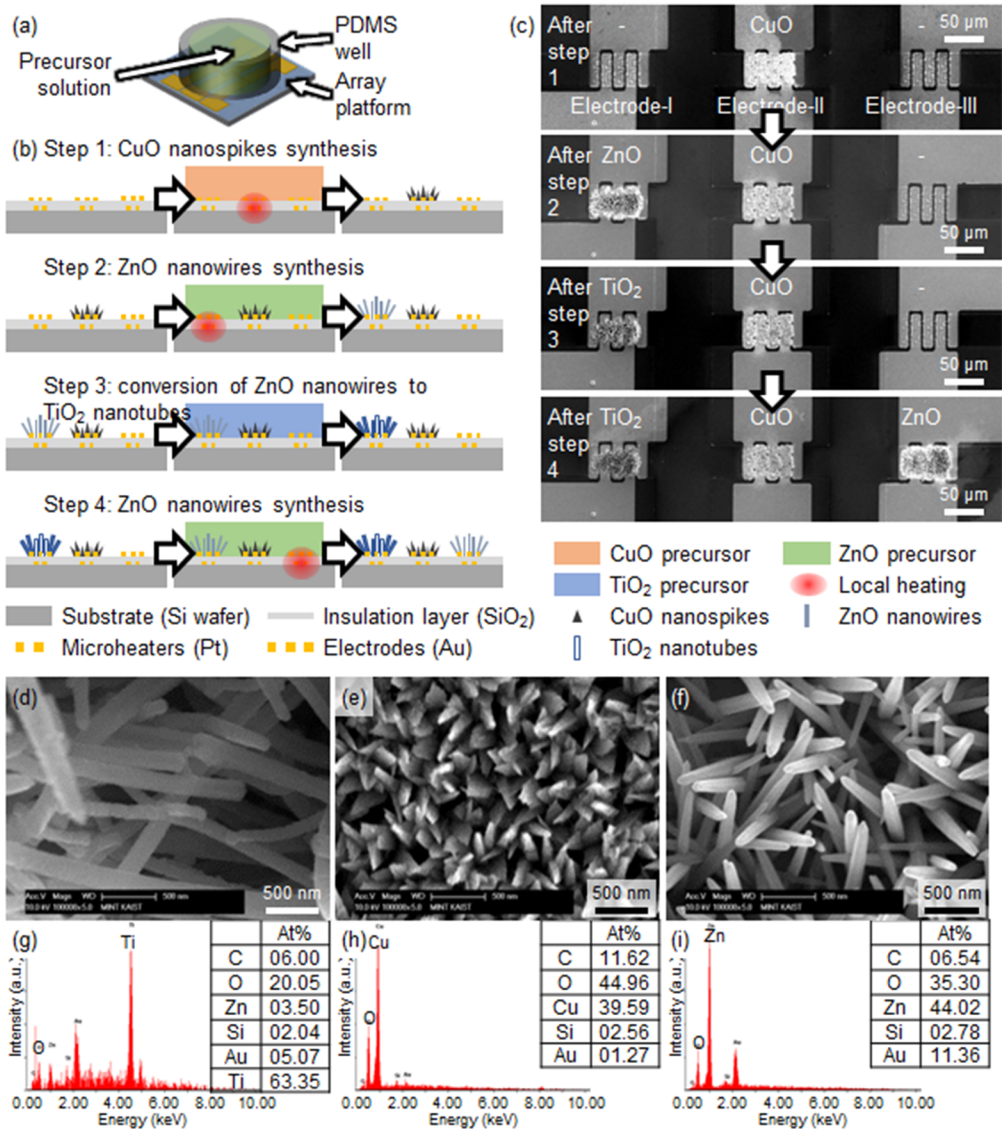

Figure 4. Fabrication of heterogeneous nanomaterial array: (a) Schematic of fabrication setup; (b) Process flow of the nanomaterial array fabrication: CuO nanospike synthesis on microheater 2, ZnO nanowire synthesis on microheater 1, conversion of ZnO nanowires to TiO_2 nanotubes on microheater 1 and ZnO nanowire synthesis on microheater 3; (c) SEM images of the nanomaterial array in the synthesis sequence: CuO nanowires on on microheater 2 after step 1, ZnO nanowires on microheater 1 after step 2, TiO_2 nanotubes on microheater 1 after step 3 and ZnO nanowires on microheater 3 after step 4. High resolution SEM images and EDS data of (d, g) TiO_2 nanotubes, (e, h) CuO nanospikes, and (f, i) ZnO nanowires on the array device show that different nanomaterials were successfully synthesized without detectable cross-contamination.

materials is decreased.[41,42] Because of these contrasting sensing responses, the device composed of both n-type (i.e., TiO_2 nanotube and ZnO nanowire) and p-type (i.e., CuO nanospike) nanomaterials are useful to detect both oxidizing gases, reducing gases and their mixtures.[43,44] In addition, the junction of semiconductor material and metal electrode plays an important role to determine the gas sensing characteristics. The work function of n-type materials (ZnO and TiO_2) are lower than that of metal (gold) electrode and that of p-type materials (CuO) is higher than that of metal (gold) electrode. Therefore, the materials should show Schottky contact.[45−47] However, the current−voltage (I−V) curves of sensor materials indicate very weak Schottky contacts (Figure 5a−c). These behaviors can be explained by Fermi level pinning caused by defects in the sensing materials. Because of the high densities of energy states in the band gap at the metal−semiconductor interface, the affinity rule is no longer valid and the Schottky barrier height is smaller than energy difference between work function of metal and electron affinity of semiconductor.[48−50] The energy state densities of the semiconductor materials can be verified by measuring the absorbance of the materials. The bandgaps of TiO_2, CuO, and ZnO are 3.2,[51] 1.2,[52] and 3.37 eV,[53] respectively, which correspond to the wavelengths of λ = 387, 1033, and 367 nm, respectively. The absorbance-wavelength curves indicate that significant amount of visible light is absorbed by the TiO_2 nanotubes, ZnO nanowires and CuO nanospikes (see Supporting Information Figure S6a−c). These absorption spectra appear to originate from detects between conduction and valence bands of the materials.[52,54,55] These defects were generated by hydrothermal and LPD processes and made weak Schottky contacts by increasing the densities of energy states.

Another crucial factor for the sensor response is the junction between sensing materials.[56] Numerous junctions are formed

DOI: 10.1021/acsami.5b00110
ACS Appl. Mater. Interfaces 2015, 7, 10152−10161

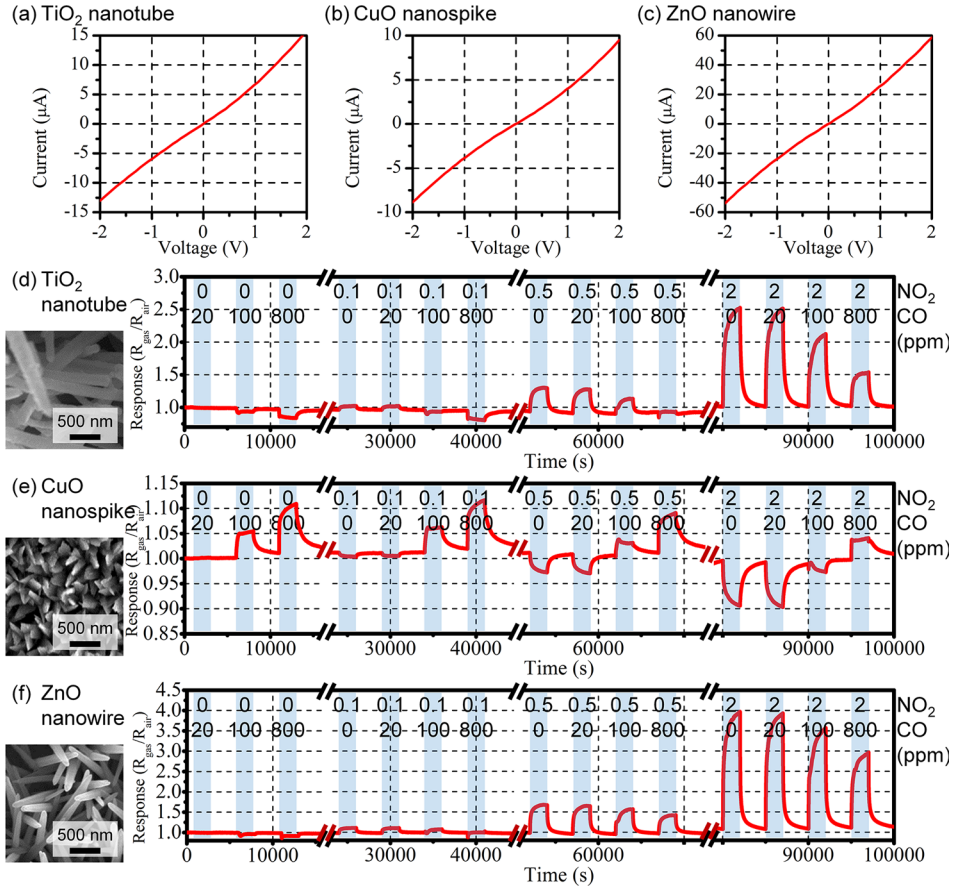

Figure 5. Current−voltage curves of (a) TiO_2 nanotube, (b) CuO nanospike, and (c) ZnO nanowire array. Sensing responses of (d) TiO_2 nanotube, (e) CuO nanospike, and (f) ZnO nanowire arrays to various mixture of 0−2 ppm of NO_2 gas and 0−800 ppm of CO gas. N-type semiconductors (TiO_2 nanotubes and ZnO nanowires) show increasing resistance in oxidizing gas (NO_2) and decreasing resistance in reducing gas (CO). P-type semiconductor (CuO nanospikes) exhibit the opposite response patterns.

between synthesized nanomaterials during the synthesis process. For example, ZnO nanowires grown on the interdigitated electrode form numerous junctions (see Supporting Information Figure S6d). When a ZnO nanowire meet another nanowire on its growth direction, two nanowires are first interconnected but continuously grow along their own crystalline growth directions. These nanowire junctions generate potential barriers that play crucial roles to enhance the sensitivity to the target gases.[56] For example, in n-type materials, the junctions have high electrical resistances in the atmospheric condition by capturing oxygen molecules as negatively charged oxygen ions. The potential barriers of junctions are dramatically increased or decreased by reacting with oxidizing (e.g., NO_2) or reducing (e.g., CO) gases, respectively. The concentrations of each component in mixture gas can be determined by combining and analyzing multiple data from each sensing material. The sensing tests were conducted for multicomponent gases consisting of 0−2 ppm of NO_2 and 0−800 ppm of CO gases, which are comparable to the air quality guidelines (exposure for 1 h) by World Health Organization (WHO).[57,58] Figures 5d−f shows the responses of multiplexed sensor consisting of three nanomaterials to multicomponent gases. Here, the response was defined as $S = R_{gas}/R_0 = 1 + (\Delta R/R_0)$, where R_0, R_{gas}, and ΔR represent the baseline resistance in ambient condition, the resistance during target gas exposure and the change of resistance by the exposure to target gas, respectively. It is well-known that the resistance of n-type materials is increased with increasing concentration of oxidizing gas (e.g., NO_2) and decreased with increasing concentration of reducing gas (e.g., CO).[36,38,39,41,42] On the other hand, the resistances of p-type materials show the opposite behavior to oxidizing or reducing gases.[36,37,40,59,60]

The empirical and theoretical investigations have confirmed that the relative changes of resistances of semiconducting metal oxide materials by single target gas are nonlinear power functions of its partial pressure (i.e., $\Delta R/R_0 = aP^n$, where P is the partial pressure of the target gas and a and n are real constants).[61,62] However, the response to multicomponent gas analytes has not been well studied due to the nonlinear relationship between response and partial pressure, and the interaction between analyte gases that complicates the sensor response.[62] Both NO_2 and CO gases react with the sensing material and they also can react with each other in the air.[63−65] However, only the surface reactions were considered in this work because the reaction between NO_2 and CO gases can be ignored due to their low concentrations.[64,65] The empirical equations for the sensor response were determined by using multiple data of response versus gas concentrations (as shown in Supporting Information Figure S7). Six equations (Supporting Information eqs S1−6) were obtained by using three kinds of sensing materials (TiO_2 nanotubes, CuO nanospikes, and ZnO nanowires) and two kinds of target gases (CO and NO_2). The equations for the sensor responses to multicomponent gas were obtained by multiplying two equations for different gas

DOI: 10.1021/acsami.5b00110
ACS Appl. Mater. Interfaces 2015, 7, 10152−10161

analytes because six equations were derived from the same gas sensing mechanism (i.e., adsorption and desorption of oxygen molecules on the surface of the nanomaterials) and they are individual state functions.[66] Three integrated equations for different sensing materials (eqs 1−3) can be obtained as listed below (see Supporting Information for details about finding the relationships between response and concentration)

$$S_{TiO_2} = [1 + \{628900 \cdot (P_{NO_2}/P_{atm})^{1}\}] \cdot [1 + \{-12.84 \cdot (P_{CO}/P_{atm})^{0.5435}\}] \quad (1)$$

$$S_{CuO} = [1 + \{-15700 \cdot (P_{NO_2}/P_{atm})^{0.9268}\}] \cdot [1 + \{4.106 \cdot (P_{CO}/P_{atm})^{0.4888}\}] \quad (2)$$

$$S_{ZnO} = [1 + \{1346000 \cdot (P_{NO_2}/P_{atm})^{1}\}] \cdot [1 + \{-7.324 \cdot (P_{CO}/P_{atm})^{0.5444}\}] \quad (3)$$

Three equations listed above can be used for the estimation of unknown concentrations of CO and NO_2 gases in their mixture by graphical solution to overdetermined nonlinear simultaneous equations.[65] To demonstrate the validity of this method, we have tested the gas sensors for two different mixture gases (sample gas I [NO_2] = 0.2 ppm, [CO] = 50 ppm; sample gas II [NO_2] = 0.2 ppm, [CO] = 400 ppm). Figure 6a and b shows the response of multiplexed gas sensor to the sample gases I and II. The average responses of the TiO_2 nanotubes, CuO nanospikes and ZnO nanowires were 1.066, 1.022, and 1.209 to sample gas I and 0.868, 1.076, and 1.121 to sample gas II, respectively. Three curves for NO_2 versus CO concentrations corresponding to the measured response of TiO_2 nanotubes, CuO nanospikes, and ZnO nanowires were first obtained as shown in Figure 6c. Although three curves for each sensor should intersect at the same point in an ideal situation, they intersect with each other at three different points since the equations were formulated by empirical method with experimental results, in which a certain levels of errors can be involved. Therefore, we have instead taken the incenter of triangle formed by these three individual intersection points as the estimated concentrations of NO_2 and CO in the mixture gas. The method proposed in this work is composed of three convergence process to calculate the intersection points and simple calculation to obtain the incenter of these intersection points. This simple analysis method can be suitable for real-time, portable gas sensor applications that require fast and simple calculation for the quick estimation of gas concentrations. As shown in Figure 6d and e, the concentrations of NO_2 and CO gases in the sample gas I were estimated as 0.186 and 39.00 ppm, respectively. The errors between the estimated and real concentrations were 7.12% and 22.00% for NO_2 and CO gases, respectively. By using the same method, the concentrations of NO_2 and CO gases in sample gas II were estimated as 0.164 and 438.9 ppm, respectively. In this case, the relative errors were 17.76% and 9.73% for NO_2 and CO gases, respectively. (see Supporting Information for details about estimating the concentrations of NO_2 and CO gases) These errors might be due to the instability of sensor, inaccurate fitting or possible reaction between NO_2 and CO gases. These error can be reduced by using more stable and reliable sensing materials and by larger number of gas tests for more accurate extraction of empirical equations. Nonetheless, this approach

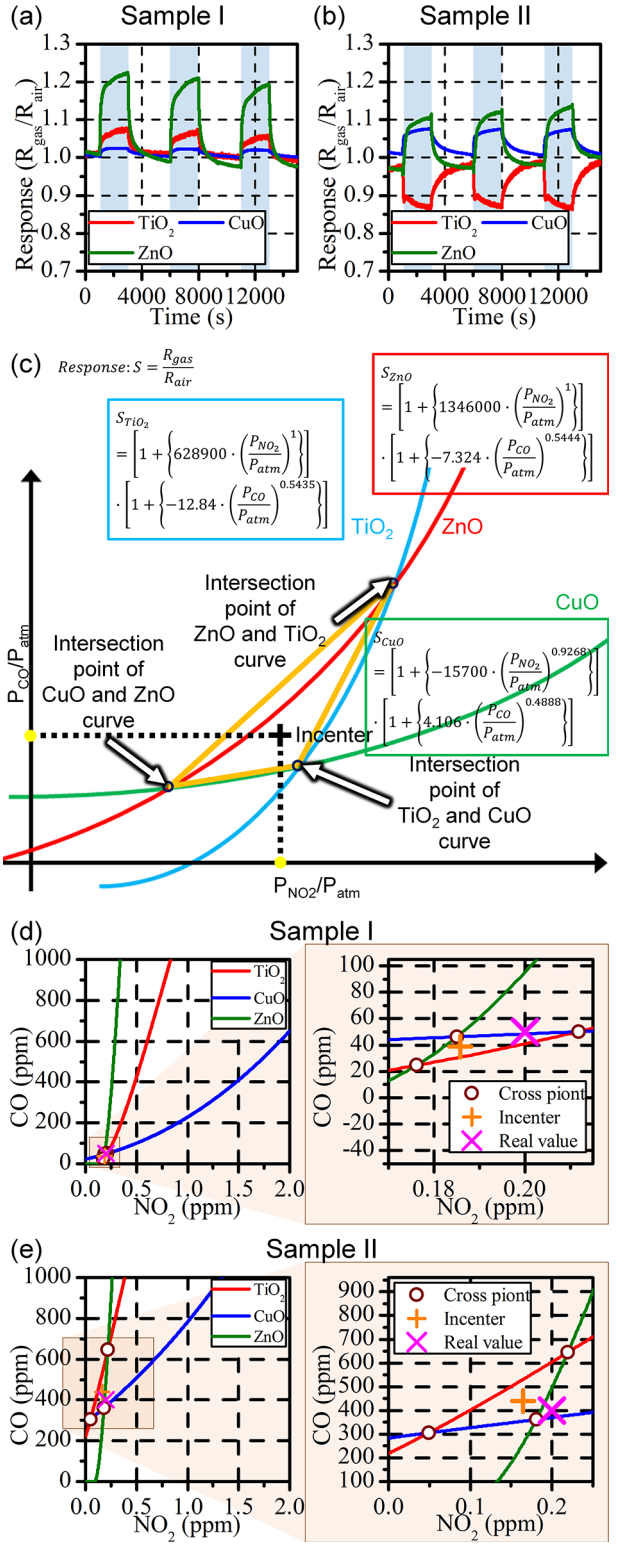

Figure 6. Estimation of mixture gas concentrations by graphical solution: (a, b) sensing responses of array of TiO_2 nanotubes, CuO nanospikes, and ZnO nanowires to the mixture of NO_2 and CO gases ((a) sample I, 0.2 ppm of NO_2 and 50 ppm of CO; (b) sample II, 0.2 ppm of NO_2 and 400 ppm of CO). (c) Schematics of concentration estimation process. The inset of the three intersection points of the three curves from three sensing materials is considered as the concentrations of individual gases in their mixture. (d, e) Calculation of concentrations of NO_2 and CO gases in sample gas I (d) and II (e).

DOI: 10.1021/acsami.5b00110
ACS Appl. Mater. Interfaces 2015, 7, 10152−10161

provides very simple method to the estimation of individual gas concentrations in the mixture gas with reasonable accuracy.

CONCLUSIONS

In summary, we have developed a novel and facile fabrication method for the heterogeneous nanomaterial array by using sequential combinations of localized hydrothermal and LPD reaction processes in different liquid chemical environments. This method enables the fabrication of highly integrated array of different nanomaterials within a sub-500-μm region on a single device chip by simple and low-cost process. The device demonstrated sensitive gas sensing performance under subppm of NO_2 gas and tens of parts per million of CO gas. Furthermore, we could determine the concentrations of NO_2 and CO gases in the mixture gas by analyzing data from the three sensing materials via graphical method of overdetermined simultaneous nonlinear equations. The fabrication technology developed here allows selective synthesis and direct integration of multiple functional nanomaterials with less power and material consumption. Although we have only demonstrated the gas sensor array of ZnO nanowires, CuO nanospikes and TiO_2 nanotubes in this work, this method will be applicable to the fabrication of multiplexed array of numerous nanomaterials. Furthermore, it is expected that this technology can be widely used for not only gas sensors but also for various kinds of functional nanodevices such as biochemical sensors, electronic devices or optical devices that require highly integrated heterogeneous nanomaterial array.

ASSOCIATED CONTENT

Supporting Information

Details of microheater device, synthesis process of nanomaterials, analysis of local heating, fabrication of heterogeneous nanomaterial array, and mixture gas sensing. The Supporting Information is available free of charge on the ACS Publications website at DOI: 10.1021/acsami.5b00110.

AUTHOR INFORMATION

Corresponding Author

*E-mail: inkyu@kaist.ac.kr.

Author Contributions

The manuscript was written through contributions of all authors. All authors have given approval to the final version of the manuscript.

Funding

Center for Integrated Smart Sensors funded by the Ministry of Education, Science and Technology as Global Frontier Project (CISS-2012-M3A6A6054201) and Nano·Material Technology Development Program through the National Research Foundation of Korea (NRF) funded by the Ministry of Education, Science, ICT & Future Planning (No. 2013043661).

Notes

The authors declare no competing financial interest.

REFERENCES

(1) Seiyama, T.; Kato, A.; Fujiishi, K.; Nagatani, M. A New Detector for Gaseous Components Using Semiconductive Thin Films. *Anal. Chem.* **1962**, *34*, 1502−1503.

(2) Taguchi, N. Jpn. Patent 45-38200, 1962.

(3) Eranna, G.; Joshi, B. C.; Runthala, D. P.; Gupta, R. P. Oxide Materials for Development of Integrated Gas Sensors—A Comprehensive Review. *Crit. Rev. Solid State Mater. Sci.* **2004**, *29*, 111−188.

(4) Barsan, N.; Koziej, D.; Weimar, U. Metal Oxide-Based Gas Sensor Research: How to? *Sens. Actuators, B* **2007**, *121*, 18−35.

(5) Kim, S.-J.; Hwang, I.-S.; Kang, Y. C.; Lee, J.-H. Design of Selective Gas Sensors Using Additive-Loaded In_2O_3 Hollow Spheres Prepared by Combinatorial Hydrothermal Reactions. *Sensors* **2011**, *11*, 10603−10614.

(6) Capone, S.; Forleo, A.; Francioso, L.; Rella, R.; Siciliano, P.; Spadavecchia, J.; Presicce, D. S.; Taurino, A. M. Solid State Gas Sensors: State of the Art and Future Activities. *J. Optoelectron. Adv. Mater.* **2003**, *5*, 1335−1348.

(7) Morrison, S. R. Selectivity in Semiconductor Gas Sensors. *Sensor. Actuator.* **1987**, *12*, 425−440.

(8) Cabot, A.; Arbiol, J.; Cornet, A.; Morante, J. R.; Chen, F.; Liu, M. Mesoporous Catalytic Filters for Semiconductor Gas Sensors. *Thin Solid Films* **2003**, *436*, 64−69.

(9) Zhan, Z.; Jiang, D.; Xu, J. Investigation of a New In_2O_3-Based Selective H_2 Gas Sensor with Low Power Consumption. *Mater. Chem. Phys.* **2005**, *90*, 250−254.

(10) Persaud, K.; Dodd, G. Analysis of Discrimination Mechanisms in the Mammalian Olfactory System Using a Model Nose. *Nature* **1982**, *299*, 352−355.

(11) Srivastava, A. K. Detection of Volatile Organic Compounds (VOCs) Using SnO_2 Gas-Sensor Srray and Artificial Neural Network. *Sens. Actuators, B* **2003**, *96*, 24−37.

(12) McAlpine, M. C.; Ahmad, H.; Wang, D.; Heath, J. R. Highly Ordered Nanowire Arrays on Plastic Substrates for Ultrasensitive Flexible Chemical Sensors. *Nat. Mater.* **2007**, *6*, 379−384.

(13) Kwon, H.-J.; Kim, D.-G.; Hong, K.-S. Multiple Odor Recognition and Source Direction Estimation with an Electronic Nose System. *Int. J. Distrib. Sens. N.* **2013**, *2013*, 361378.

(14) Aishima, T. Aroma Discrimination by Pattern-Recognition Analysis of Responses from Semiconductor Gas Sensor Array. *J. Agr. Food. Chem.* **1991**, *39*, 752−756.

(15) Gardner, J. W.; Shurmer, H. V.; Tan, T. T. Application of an Electronic Nose to the Discrimination of Coffees. *Sens. Actuators, B* **1992**, *6*, 71−75.

(16) Wang, C.; Yin, L.; Zhang, L.; Xiang, D.; Gao, R. T. Metal Oxide Gas Sensors: Sensitivity and Influencing Factors. *Sensors* **2010**, *10*, 2088−2106.

(17) Chen, X.; Wong, C. K. Y.; Yuan, C. A.; Zhang, G. Nanowire-Based Gas Sensors. *Sens. Actuators, B* **2013**, *177*, 178−195.

(18) Xie, C.; Xiao, L.; Hu, M.; Bai, Z.; Xia, X.; Zeng, D. Fabrication and Formaldehyde Gas-Sensing Property of ZnO-MnO_2 Coplanar Gas Sensor Arrays. *Sens. Actuators, B* **2010**, *145*, 457−463.

(19) Li, B.; Santhanam, S.; Schultz, L.; Jeffries-EL, M.; Iovu, M. C.; Sauvé, G.; Cooper, J.; Zhang, R.; Revelli, J. C.; Kusne, A. G.; et al. Inkjet Printed Chemical Sensor Array Based on Polythiophene Conductive Polymers. *Sens. Actuators, B* **2007**, *123*, 651−660.

(20) Briand, D.; Colin, S.; Courbat, J.; Raible, S.; Kappler, J.; de Rooij, N. F. Integration of MOX Gas Sensors on Polyimide Hotplates. *Sens. Actuators, B* **2008**, *130*, 430−435.

(21) Leiterer, C.; Broenstrup, G.; Jahr, N.; Urban, M.; Arnold, C.; Christiansen, S.; Fritzsche, W. Applying Contact to Individual Silicon Nanowires Using a Dielectrophoresis (DEP)-Based Technique. *J. Nanopart. Res.* **2013**, *15*, 1628.

(22) Hsieh, G.-W.; Wang, J.; Ogata, K.; Robertson, J.; Hofmann, S.; Milne, W. I. Stretched Contact Printing of One-Dimensional Nanostructures for Hybrid Inorganic−Organic Field Effect Transistors. *J. Phys. Chem. C* **2012**, *116*, 7118−7125.

(23) Sim, J.; Choi, J.; Kim, J. Humidity Sensing Characteristics of Focused Ion Beam-Induced Suspended Single Tungsten Nanowire. *Sens. Actuators, B* **2014**, *194*, 38−44.

(24) Li, D.; Leung, Y. H.; Djurišić, A. B.; Liu, Z. T.; Xie, M. H.; Gao, J.; Chan, W. K. CuO Nanostructures Prepared by a Chemical Method. *J. Cryst. Growth* **2005**, *282*, 105−111.

(25) Li, Q. C.; Kumar, V.; Li, Y.; Zhang, H. T.; Marks, T. J.; Chang, R. P. H. Fabrication of ZnO Nanorods and Nanotubes in Aqueous Solutions. *Chem. Mater.* **2005**, *17*, 1001−1006.

DOI: 10.1021/acsami.5b00110
ACS Appl. Mater. Interfaces 2015, 7, 10152−10161

(26) Deki, S.; Aoi, Y.; Hiroi, O.; Kajinami, A. Titanium(IV) Oxide Thin Films Prepared from Aqueous Solution. *Chem. Lett.* **1996**, 433−434.
(27) Arafat, M. M.; Dinan, B.; Akbar, S. A.; Haseeb, A. S. Gas Sensors Based on One Dimensional Nanostructured Metal-Oxides: A Review. *Sensors* **2012**, *12*, 7207−7258.
(28) Rajasekaran, S. *Numerical Methods in Science and Engineering: A Practical Approach*; S Chand & Co Ltd; New Delhi, India, 2003; pp 236−312.
(29) Yang, Z.; Liu, Q. H.; Yang, L. The Effects of Addition of Citric Acid on the Morphologies of ZnO Nanorods. *Mater. Res. Bull.* **2007**, *42*, 221−227.
(30) Zhou, Y.; Wu, W. B.; Hu, G. D.; Wu, H. T.; Cui, S. G. Hydrothermal Synthesis of ZnO Nanorod Arrays with the Addition of Polyethyleneimine. *Mater. Res. Bull.* **2008**, *43*, 2113−2118.
(31) Kusiak, A.; Battaglia, J.-L.; Gomez, S.; Manaud, J.-P.; Lepetitcorps, Y. CuO Thin Films Thermal Conductivity and Interfacial Thermal Resistance Estimation. *Eur. Phys. J.: Appl. Phys.* **2006**, *35*, 17−27.
(32) Vaseem, M.; Umar, A.; Kim, S. H.; Hahn, Y.-B. Low-Temperature Synthesis of Flower-Shaped CuO Nanostructures by Solution Process: Formation Mechanism and Structural Properties. *J. Phys. Chem. C* **2008**, *112*, 5729−5735.
(33) Sun, Y.; George Ndifor-Angwafor, N.; Jason Riley, D.; Ashfold, M. N. R. Synthesis and Photoluminescence of Ultra-Thin ZnO Nanowire/Nanotube Arrays Formed by Hydrothermal Growth. *Chem. Phys. Lett.* **2006**, *431*, 352−357.
(34) Jin, C. Y.; Li, Z.; Williams, R. S.; Lee, K.-C.; Park, I. Localized Temperature and Chemical Reaction Control in Nanoscale Space by Nanowire Array. *Nano Lett.* **2011**, *11*, 4818−4825.
(35) Chien, H.-C.; Yao, D.-J.; Huang, M.-J.; Chang, T.-Y. Thermal Conductivity Measurement and Interface Thermal Resistance Estimation Using SiO_2 Thin Film. *Rev. Sci. Instrum.* **2008**, *79*, 054902.
(36) Fine, G. F.; Cavanagh, L. M.; Afonja, A.; Binions, R. Metal Oxide Semi-Conductor Gas Sensors in Environmental Monitoring. *Sensors* **2010**, *10*, 5469−5502.
(37) Kim, H.-J.; Lee, J.-H. Highly Sensitive and Selective Gas Sensors Using P-Type Oxide Semiconductors: Overview. *Sens. Actuators, B* **2014**, *192*, 607−627.
(38) Oh, E.; Choi, H.-Y.; Jung, S.-H.; Cho, S.; Kim, J. C.; Lee, K.-H.; Kang, S.-W.; Kim, J.; Yun, J.-Y.; Jeong, S.-H. High-Performance NO_2 Gas Sensor Based on ZnO Nanorod Grown by Ultrasonic Irradiation. *Sens. Actuators, B* **2009**, *141*, 239−243.
(39) Zhuo, Y.; Huang, L.; Ling, Y.; Li, H.; Wang, J. A Novel NO_2 Sensor Based on TiO_2 Nanotubes Array with In-Situ Au Decoration. *J. Nanosci. Nanotechnol.* **2013**, *13*, 1177−1181.
(40) Das, A.; Venkataramana, B.; Partheephan, D.; Prasad, A. K.; Dhara, S.; Tyagi, A. K. Facile Synthesis of Nanostructured CuO for Low Temperature NO_2 Sensing. *Phys. E (Amsterdam, Neth.)* **2013**, *54*, 40−44.
(41) Liu, C.-Y.; Chen, C.-F.; Leu, J.-P. Fabrication and CO Sensing Properties of Mesostructured ZnO Gas Sensors. *J. Electrochem. Soc.* **2009**, *156*, J16−J19.
(42) Park, J.-A.; Moon, J.; Lee, S.-J.; Kim, S. H.; Zyung, T.; Chu, H. Y. Structure and CO gas Sensing Properties of Electrospun TiO_2 Nanofibers. *Mater. Lett.* **2010**, *64*, 255−257.
(43) Liu, X.; Cheng, S.; Liu, H.; Hu, S.; Zhang, D.; Ning, H. A Survey on Gas Sensing Technology. *Sensors* **2012**, *12*, 9635−9665.
(44) Wöllenstein, J.; Plaza, J. A.; Cané, C.; Min, Y.; Böttner, H.; Tuller, H. L. A Novel Single Chip Thin Film Metal Oxide Array. *Sens. Actuators, B* **2003**, *93*, 350−355.
(45) Pierret, R. F. *Semiconductor Device Fundamentals*; Addison-Wesley; Boston, 1996; pp 477−504.
(46) Singh, N.; Yan, C.; Lee, P. S.; Comini, E. Sensing Properties of Different Classes of Gases Based on the Nanowire-Electrode Junction Barrier Modulation. *Nanoscale* **2011**, *3*, 1760−1765.
(47) Wei, T.-Y.; Yeh, P.-H.; Lu, S.-Y.; Wang, Z. L. Gigantic Enhancement in Sensitivity Using Schottky Contacted Nanowire Nanosensor. *J. Am. Chem. Soc.* **2009**, *131*, 17690−17695.
(48) Brillson, L. J.; Lu, Y. ZnO Schottky Barriers and Ohmic Contacts. *J. Appl. Phys.* **2011**, *109*, No. 121301.
(49) Cohen, M. L. Schottky and Bardeen Limits for Schottky Barriers. *J. Vac. Sci. Technol.* **1979**, *16*, 1135−1136.
(50) Janotti, A.; Van De Walle, C. G. Fundamentals of Zinc Oxide as a Semiconductor. *Rep. Prog. Phys.* **2009**, *72*, No. 126501.
(51) Tang, H.; Berger, H.; Schmid, P. E.; Lévy, F.; Burri, G. Photoluminescence in TiO_2 Anatase Single Crystals. *Solid State Commun.* **1993**, *87*, 847−850.
(52) Abdel Rafea, M.; Roushdy, N. Determination of the Optical Band Gap for Amorphous and Nanocrystalline Copper Oxide Thin Films Prepared by SILAR Technique. *J. Phys. D: Appl. Phys.* **2009**, *42*, No. 015413.
(53) Bai, S.; Wu, W.; Qin, Y.; Cui, N.; Bayerl, D. J.; Wang, X. High-Performance Integrated ZnO Nanowire UV Sensors on Rigid and Flexible Substrates. *Adv. Funct. Mater.* **2011**, *21*, 4464−4469.
(54) Jiao, Z.; Chen, T.; Xiong, J.; Wang, T.; Lu, G.; Ye, J.; Bi, Y. Visible-Light-Driven Photoelectrochemical and Photocatalytic Performances of Cr-Doped $SrTiO_3/TiO_2$ Heterostructured Nanotube Arrays. *Sci. Rep.* **2013**, *3*, 2720.
(55) Fletcher, C.; Jiang, Y.; Sun, C.; Amal, R. Morphological Evolution and Electronic Alteration of ZnO Nanomaterials Induced by Ni/Fe Co-Doping. *Nanoscale* **2014**, *6*, 7312−7318.
(56) Ahn, M.-W.; Park, K.-S.; Heo, J.-H.; Kim, D.-W.; Choi, K. J.; Park, J.-G. On-Chip Fabrication of ZnO-Nanowire Gas Sensor with High Gas Sensitivity. *Sens. Actuators, B* **2009**, *138*, 168−173.
(57) World Health Organization. *Air Quality Guidelines for Particulate Matter, Ozone, Nitrogen Dioxide and Sulfur Dioxide*; World Health Organization: Geneva, 2006.
(58) World Health Organization. *Guidelines for Air Quality*; World Health Organization: Geneva, 2000.
(59) Aslani, A.; Oroojpour, V. CO Gas Sensing of CuO Nanostructures, Synthesized by an Assisted Solvothermal Wet Chemical Route. *Phys. B (Amsterdam, Neth.)* **2011**, *406*, 144−149.
(60) Liao, L.; Zhang, Z.; Yan, B.; Zheng, Z.; Bao, Q. L.; Wu, T.; Li, C. M.; Shen, Z. X.; Zhang, J. X.; Gong, H.; et al. Multifunctional CuO Nanowire Devices: P-Type Field Effect Transistors and CO Gas Sensors. *Nanotechnology* **2009**, *20*, No. 085203.
(61) Yamazoe, N.; Shimanoe, K. Theory of Power Laws for Semiconductor Gas Sensors. *Sens. Actuators, B* **2008**, *128*, 566−573.
(62) Clifford, P. K.; Tuma, D. T. Characteristics of Semiconductor Gas Sensors I. Steady State Gas Response. *Sensor. Actuator.* **1982**, *3*, 233−254.
(63) Burcat, A.; Lifshitz, A. Kinetics of The Reaction $NO_2 + CO \rightarrow NO + CO_2$ Single-Pulse Shock Tube Studies. *J. Phys. Chem.* **1970**, *74*, 263−268.
(64) Brown, F. B.; Crist, R. H. Further Studies on the Oxidation of Nitric Oxide: The Rate of the Reaction Between Carbon Monoxide and Nitrogen Dioxide. *J. Phys. Chem.* **1941**, *9*, 840−846.
(65) Johnston, H. S.; Bonner, W. A.; Wilson, D. J. Carbon Isotope Effect During Oxidation of Carbon Monoxide with Nitrogen Dioxide. *J. Phys. Chem.* **1957**, *26*, 1002−1006.
(66) Schierbaum, K. D.; Weimar, U.; Göpel, W. Multicomponent Gas Analysis: An Analytical Chemistry Approach Applied to Modified SnO_2 Sensors. *Sens. Actuators, B* **1990**, *2*, 71−78.

DOI: 10.1021/acsami.5b00110
ACS Appl. Mater. Interfaces 2015, 7, 10152−10161